arXiv:1505.07942v1 [cond-mat.mtrl-sci] 29 May 2015

Impact of oxygen doping and oxidation state of iron on the electronic and magnetic properties of $BaFeO_{3-\delta}$

I. V. Maznichenko,[1,*] S. Ostanin,[2] L. V. Bekenov,[3] V. N. Antonov,[3,2] I. Mertig,[1,2] and A. Ernst[2]

[1] *Institut für Physik, Martin-Luther-Universität Halle-Wittenberg, D-06099 Halle, Germany*
[2] *Max-Planck-Institut für Mikrostrukturphysik, Weinberg 2, D-06120 Halle, Germany*
[3] *Institute of Metal Physics, Vernadsky Street 36, 03142 Kiev, Ukraine*

(Dated: June 1, 2015)

We studied structural, electronic and magnetic properties of a cubic perovskite $BaFeO_{3-\delta}$ ($0 \leq \delta \leq 0.5$) within the density functional theory using a generalized gradient approximation and a GGA+U method. According to our calculations, $BaFeO_3$ in its stoichiometric cubic structure should be half-metallic and strongly ferromagnetic, with extremely high Curie temperature (T_C) of 700 – 900 K. However, a such estimate of T_C disagrees with all available experiments, which report that T_C of the $BaFeO_3$ and undoped $BaFeO_{3-\delta}$ films varies between 111 K and 235 K or, alternatively, that no ferromagnetic order was detected there. Fitting the calculated x-ray magnetic circular dichroism spectra to the experimental features seen for $BaFeO_3$, we concluded that the presence of oxygen vacancies in our model enables a good agreement. Thus, the relatively low T_C measured in $BaFeO_3$ can be explained by oxygen vacancies intrinsically presented in the material. Since iron species near the O vacancy change their oxidation state from 4+ to 3+, the interaction between Fe^{4+} and Fe^{3+}, which is antiferromagnetic, weakens the effective magnetic interaction in the system, which is predominantly ferromagnetic. With increasing δ in $BaFeO_{3-\delta}$, its T_C decreases down to the critical value when the magnetic order becomes antiferromagnetic. Our calculations of the electronic structure of $BaFeO_{3-\delta}$ illustrate how the ferromagnetism originates and also how one can keep this cubic perovskite robustly ferromagnetic far above the room temperature.

PACS numbers: 78.20.Ls, 75.50.Bb, 75.30.Mb

I. INTRODUCTION

A multiferroic tunnel junction, in which a robustly ferroelectric barrier, such as $PbTiO_3$ or $BaTiO_3$, is grown epitaxially between two ferromagnetic electrodes, allows to tune the spin transport by switching the magnetization of an electrode. Additionally, the barrier polarization reversal can change the interfacial magnetoelectric coupling and, thus, the four-state tunneling resistance can be detected.[1,2] As for the upper electrode, the Fe and Co films can be easily grown on the TiO_2 terminated polar perovskites,[3] while the best bottom-electrode material, which can be used here as the substrate, must satisfy the following conditions: (i) its structure should be in a good lattice match with ferroelectrics and (ii) the electrode material should be robustly ferromagnetic with relatively high Curie temperature (T_C). A very good choice would be a magnetic perovskite since a ferroelectric can be well grown on such substrates. In particular, perovskites ABO_3 with a magnetic cation on site B are well-known to be compatible with ferroelectrics.[4] Recently, Pantel *et al.*[5] have demonstrated the four-state tunneling resistance effect using the 3.2-nm-thick perovskite barrier $PbZr_{0.2}Ti_{0.8}O_3$ (001) grown on ferromagnetic La(Sr)MnO_3 (LSMO).

One of the possible candidates for the substrate in a multiferroic tunnel junction seems to be $BaFeO_3$ (BFO). Although bulk BFO is hexagonal, the perovskite phase can be stabilized in epitaxial films. X-ray diffraction studies show that thin BFO films grown on $SrTiO_3$(001) adopt the cubic perovskite structure with the lattice parameter of 3.97 Å.[6,7] For $BaFeO_{3-\delta}$ films, the larger lattice parameter of 4.07 Å has been measured.[8] Regarding the observed magnetic properties of the cubic BFO, such as the Fe magnetic moment, magnetic ordering and T_C, the reports seem contradictory. Callender *et al.*[9] reported that a pseudocubic BFO is robustly ferromagnetic (FM) with T_C=235 K. Instead, the oxygen deficient $BaFeO_{3-\delta}$ films exhibit antiferromagnetism (AFM) at room temperature, while a weakly ferromagnetic behavior extends above 390 K.[8] For thick BFO films, Chakraverty *et al.*[6] reported T_C=115 K and a saturation magnetization of 3.2 μ_B/f.u., which both remain stable as a function of film thickness, with no signature of the spin spiral structure up to 300 nm.

In the case of completely oxidized stoichiometric cubic BFO, the oxidation state of iron is 4+ that leads to the twofold orbitally degenerated configuration $t_{2g}^3 e_g^1$. In polyatomic molecules the half occupied e_g level have to split according to Jahn and Teller.[10] In solids the effect must be cooperative. However, for $AFeO_3$ (A = Ca, Sr, Ba) this behavior, known as the cooperative Jahn-Teller distortion, was not reported so far. Instead, it occurs in antiferromagnetic $LaMnO_3$ where up to 750 K the e_g splitting opens the band gap.[11–13] On the other hand, the Fe oxidation state in oxides is so unstable that the presence of the degenerated e_g level is not required. For instance, in metallic $CaFeO_3$ the charge disproportionaly is observed: $2Fe^{4+} \rightarrow Fe^{(4-\tau)+} + Fe^{(4+\tau)+}$, where $0 < \tau \leq 1$.[14] Thus, the issue of mixed valency might be very important in the case of BFO.

Several theoretical studies of magnetic BFO have been

recently made from first principles. For the FM order and experimental lattice parameter of the cubic BFO, the calculated magnetic moment varies between 3.0 μ_B and 3.4 μ_B per f.u.,[15,16] depending on the model approximation used to treat the exchange-correlation effects. According to the *ab initio* investigation by Ribeiro *et al.*[17] the FM solution in the stoichiometric BFO is energetically favorable against the possible AFM configurations while the FM moment is about 3.6 μ_B. A helical magnetic ordering in BFO, which is usually discussed in the context of $SrFeO_3$ and $CaFeO_3$,[18] has been investigated from first principles by Zhi Li *et al.*[19,20] The authors anticipate that the G-type helical solution can be fixed, keeping the reduced volume and, simultaneously, using the Hubbard parametrization which treats electronic correlations beyond the standard of the local density approximation. The theoretical estimations of T_C were not performed so far.

As it was already mentioned above, the Fe atoms in the BFO can have various oxidation states. The origin of this distinction in real materials can be related for instance with a particular sample preparation procedure, that can explain the large discrepancy in results of various experiments. In this work, we investigate from first-principles the impact of Fe oxidation states on structural, magnetic, optical, and electronic properties of chemically perfect BFO and $BaFeO_{3-\delta}$ ($\delta > 0$) with vacancies. The paper is organized as follows. In Section II we provide the essential details of our methods and calculations. In Section III, we present the results and discuss the structural, electronic, optical, and magnetic properties of the BFO. Finally, our summary and conclusions are drawn.

II. DETAILS OF CALCULATIONS

Our calculations of the BFO, undoped $BaFeO_{3-\delta}$, and nominally overdoped BFO were performed using a first-principles Green function method[21] based the multiple-scattering within the density functional theory in a generalized gradient approximation (GGA) to the exchange-correlation potential. [22] We used a full charge density approximation to take into account possible non-sphericity of the crystal potential and the charge density.

The Fe oxidation state was modeled using a self-interaction correction (SIC) method[23] as it is implemented within the multiple-scattering theory.[24] In this case, an oxidation state can be defined by the number of valence electrons as

$$N_{val} = Z - (N_{core} + N_{SIC}), \tag{1}$$

where Z is the total number of electrons of an isolated atom, N_{core} is the number of electrons occupying the deep energy levels and treated as the core electrons, N_{SIC} is the number of SIC corrected $3d$ electrons.

Since the SIC approach is designed only for ground state properties,[23] we used a GGA+U method[25] to take into account electronic correlation effects in calculations of exchange parameters. The later were estimated within the magnetic force theorem.[26] The critical temperature and the magnetic ordering were obtained within the Heisenberg model

$$H = -\sum_{i,j} J_{ij}\, \mathbf{e}_i \cdot \mathbf{e}_j, \tag{2}$$

where i and j label the magnetic atoms, and $\mathbf{e}_i$ is a unit vector in the direction of the magnetic moment of the ith atom. The critical temperatures were estimated using both the mean field approximation (MFA) and random phase approximation (RPA).[27] Both approaches were successfully applied to many magnetically ordered oxides including magnetic perovskites.[28,29]

Disorder effects in our study were simulated within the coherent-potential approximation (CPA).[30–32] The intrinsic oxygen vacancies in $BaFeO_{3-\delta}$ were modeled within the same CPA scheme, which implies randomly distributed vacancies over all oxygen sites. Regarding the Ba and Fe vacancies, in the literature, such cation-deficient perovskites are formally denoted as $BaFeO_{3+\delta}$, although the bulk perovskite structures are unable to accommodate interstitial oxygen.

The calculations of the XAS and XMCD were performed using the spin-polarized fully relativistic linear-muffin-tin-orbital (LMTO) method[33,34] for the experimentally observed lattice constants. The details are described in our previous papers.[35–37]

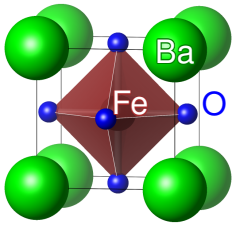

FIG. 1: (Color) The crystalline structure of the cubic $BaFeO_3$.

III. RESULTS

A. Crystalline structure of $BaFeO_3$

The ground-state phase of BFO is hexagonal with the space group symmetry $P12_1/c1$.[38] It contains six formula units (f.u.) and two types of environmentally different Fe. We calculated the structural properties using both the LDA[39] and GGA[22] to the exchange-correlation potential. The GGA (LDA) yields the equilibrium volume of 378.66 Å^3 (352.84 Å^3), which is in a good agreement with the experimental value of 388.42 Å^3. For this volume and chemically perfect BFO, we found that the AFM configuration is marginally preferable by 9 meV/f.u., as

compared to the FM solution, while the magnetic moments of each type of Fe differ significantly: 3.34 μ_B and 2.38 μ_B. The use of the electronic-correlation parameter U=2 eV applied on iron species increases the Fe magnetic moments by 12%, whereas the energy difference $\Delta E = E_{FM} - E_{AFM}$ increases up to 28 meV/f.u.

Concerning the cubic BFO phase, the LDA equilibrium lattice parameter of 3.86 Å is significantly underestimated, as compared to the experimental value of 3.97 Å, while the use of GGA results in $a = 3.963$ Å. For the latter we found that the FM ordering is strongly favorable by 110 meV/f.u. with respect to the G-type AFM configuration. Thus, we suggest that the BFO phase transformation from its hexagonal AFM to cubic FM structure goes with the volume reduction of 1.1% per f.u. and the corresponding energy barrier is 0.28 eV/f.u. In BFO films, the cubic FM phase can be stabilized at room temperature by anharmonic contributions to the free energy and/or the effects of epitaxial strain.

Thus, the crystalline structure of the hexagonal and cubic BFO can be adequately described using a conventional GGA functional. Further, we focus our study on electronic, optic, and magnetic properties of the cubic BFO phase (see Fig.1).

B. Electronic and magnetic structure of $BaFeO_3$

1. *GGA approach*

Since we found the GGA to be an appropriate functional in describing the crystalline structure of the cubic BFO, we applied the method for further study of its electronic and magnetic properties.

Within the GGA, the spin-polarized density of states (DOS) of BFO exhibits a metallic behavior in the two spin channels, as it is shown in Fig.2. This agrees with the experimental findings of Callender *et al.*,[9] who observed the ferromagnetic ordering and conductance in BFO films, annealed in the oxygen atmosphere. The iron atoms appear to have the oxidation state of 2+. Therewith, t_{2g} and e_g states are almost occupied in the majority spin channel (4.5 electrons) and only partially occupied (1.5 electrons) in the minority spin channel. The $3d$ electrons of iron experience a strong hybridization with the p states of oxygen and are widely spread over the whole valence band region. The total magnetic moment, calculated within the GGA, is 3.55 μ_B per f.u., which includes the ferromagnetically induced O moments of about 0.15 μ_B.

The exchange interaction between Fe atoms is large and positive within the GGA: 20.5 meV and 2 meV between the nearest and the next nearest neighbors, respectively. The estimated Curie temperature is about 1000 K in the mean field approximation (700 K in the random phase approximation). It has to be mentioned here that the RPA provides usually a reasonable critical temperature, while the MFA represents average exchange

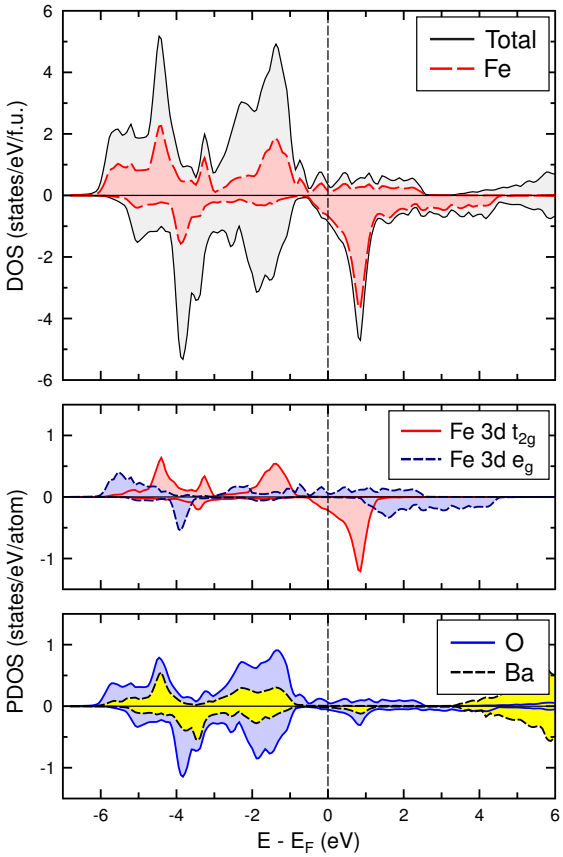

FIG. 2: (Color) The total and site-projected DOS of cubic BFO calculated within the GGA. The positive (negative) DOS values denote the majority (minority) spin states.

interaction and overestimates T_C by 30 – 40%.[40]

Thus, the Curie temperature, calculated in the cubic BFO using the GGA method, is several times larger then the experimental values (100 – 400 K). The reason is that the system is metallic within this approach and, therefore, the double exchange interaction via the oxygens and the band ferromagnetism dominate over the other exchange mechanisms, which can reduce the magnetic interaction or change its sign. Therefore, the electronic correlations, which can be substantial in oxides, must be taken into account using a more appropriate method.

2. *GGA+U approach*

At the next step, we chose the GGA+U approximation, which provides a more adequate description of oxide materials then the conventional LDA or GGA approaches.[41] Since we could not estimate the value of U from first principles, we used it as a parameter tracing the change of the electronic and magnetic properties with the value of U. In our simulations we applied the Hubbard U corrections on Fe $3d$ states and varied the value of $U_{eff} = U - J$ between 0 (here, GGA) and 9 eV. As expected, the occu-

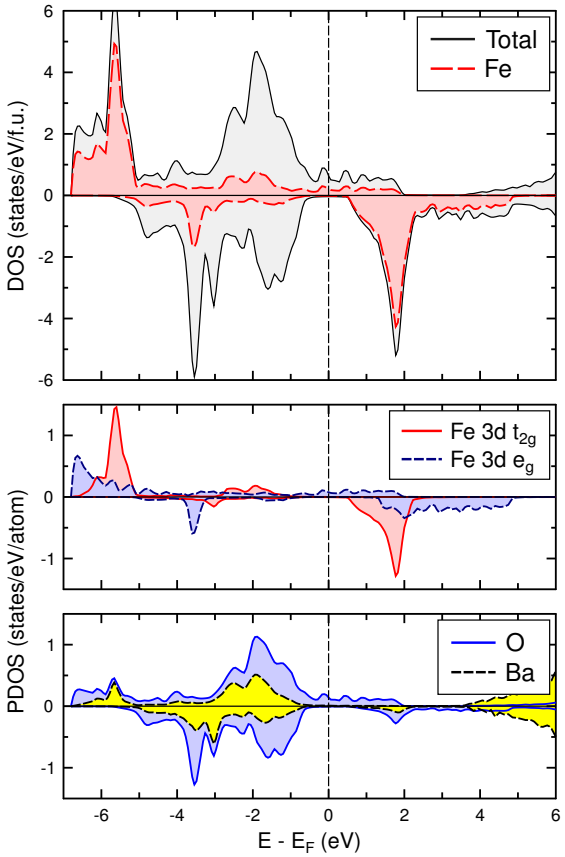

FIG. 3: (Color) The total and site-projected DOS of cubic BFO calculated within the GGA+U method with U_{eff}=3 eV.

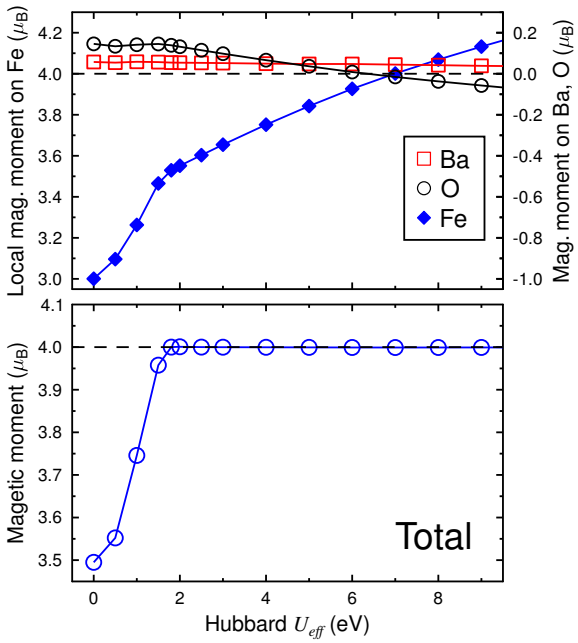

FIG. 4: (Color) The total and site-projected magnetic moments of cubic BFO calculated as a function of U. Here, $U_{eff} = 0$ means the use of GGA.

pied (unoccupied) 3d Fe states are shifted down (up) in energy on the value of $U_{eff}/2$ that opens the gap in the minority spin channel for $U_{eff} \geq 2$ eV (see the DOS in Fig.3 with $U_{eff} = 3$ eV). The size of the spin band gap depends strongly on the U_{eff} value.

In Fig.4, we show the total and all site-projected magnetic moments, which are plotted as a function of $0 \leq U_{eff} \leq 9$. The local magnetic moment of iron increases from 3 μ_B to 4.18 μ_B within the given range of U_{eff} values, while the induced magnetic moment of oxygen decreases from 0.18 μ_B to -0.08 μ_B systematically with the increase of U_{eff}. The magnetic moment induced on Ba is ≈ 0.05 μ_B and its small value changes marginally on the model variations of U. For $U_{eff} \geq 2$ eV the total moment is integer (4 μ_B/f.u), which reflects the half-metallicity of the BFO. This is larger then the experimental values of 3.2 – 3.5 μ_B/f.u., reported previously in Refs. 6,7.

As next, we calculated the exchange interaction as a function of U_{eff}. The results are presented in Fig.5. Since the BFO remains metallic within this approximation, we can classify the main magnetic interaction as the double exchange. The consequence of the strong ferromagnetic coupling is the largely overestimated T_C compared to the measured values. Although applying the GGA+U method reduces slightly the exchange interaction, mainly due to the reduction of the overlap between the Fe and oxygen states, the Curie temperature is still too high in the whole range of U_{eff}. The dependence of T_C on U_{eff} is nontrivial. First, it reduces with the increase of U_{eff}, since the Fe 3d states are getting localized and their overlap with sp states of oxygen. At $U_{eff} = 2$ eV, a band gap forms in the minority spin channel and the J^{Fe-Fe} rise up with the increase of U_{eff}. Therewith, the exchange interaction between the nearest neighbors is getting larger only until $U_{eff} \approx 4$ eV and then decreasing, while the next nearest neighbor interaction continues to increase until $U_{eff} \approx 6$ eV. As result, the Curie temperature gets up to 700 K within the RPA for $U_{eff} \approx 6$ eV and then starts to fall down. According to our estimations, the Curie temperature agrees with experimental values only for $U_{eff} > 15$ eV, which are nonphysical for this compound. Thus, consideration only electronic correlation effects does not explain magnetic properties of BFO. This fact motivated us to improve the model of BFO and make further calculations.

C. Simulation of XMCD spectra

In complex transition metal oxides, the XAS and XMCD spectra at the $L_{2,3}$ absorption edges can be used as fingerprints of the ground state. In our study we simulated the XAS and XMCD spectra varying the crystal structure, the chemical composition, the value of U_{eff}

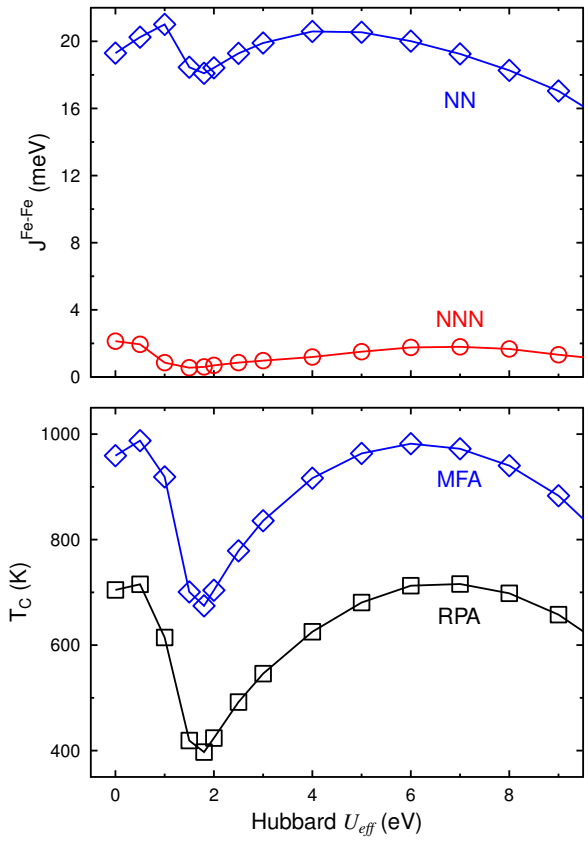

FIG. 5: (Color) Exchange interactions (upper panel) and the Curie temperature (lower panel) of the cubic BFO calculated as a function of the Hubbard parameter U_{eff} applied on the Fe 3d orbitals.

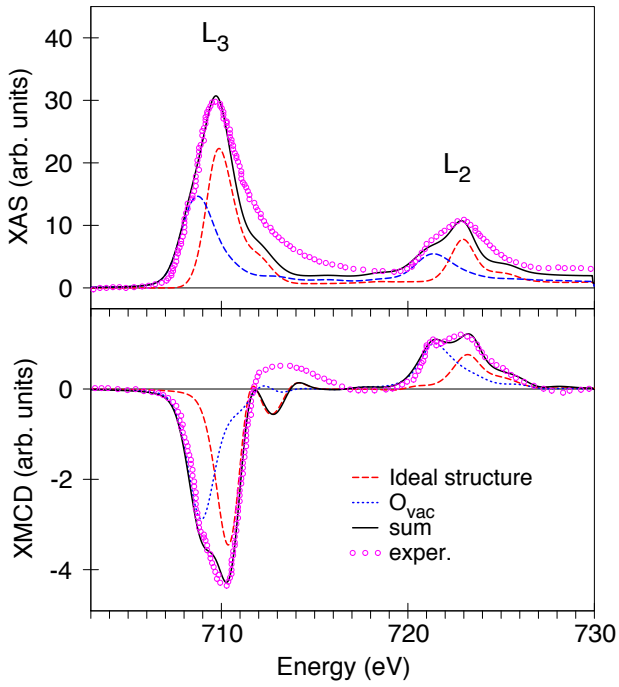

FIG. 6: (Color) Comparison between the experimental[42] x-ray absorption (upper panel) and x-ray magnetic circular dichroism (lower panel) at the Fe $L_{2,3}$ edges of $BaFeO_3$ and the spectra calculated in the GGA+U approximation (U_{eff}=3 eV) (black solid lines). Red dashed line show the spectra for ideal crystal structure, dotted blue lines present the theoretical spectra with oxygen vacancy.

for electronic correlation effects, the magnetic order, and searching for optimal agreement with available experiments.

Fig. 6 displays the experimentally measured[42] and theoretically calculated Fe $L_{2,3}$ XAS (upper panel) and XMCD (lower panel) spectra of the cubic $BaFeO_3$. The L_3 XAS spectrum exhibits a weak lower-energy shoulder at around 708 eV together with a high-energy shoulder at 713 eV. The L_2 XAS spectrum exhibits a lower-energy peak at around 721 eV. The Fe L_3 XMCD spectrum consists of major negative peak at 710 eV with low-energy shoulder and an additional positive peak at 713 eV. The Fe L_2 XMCD spectrum has double-peak structure.

First, we found the best agreement with experiments was achieved for $U_{eff} = 3$ eV. This value of U_{eff} is used later for all our calculations if it is not mentioned specifically. However, the experimental results could not explained only by taking into account strong correlations effect. For the ideal cubic BFO structure, our simulations of the XAS and XMCD spectra provide x-ray absorption intensity in the Fe L_3 only at the major peak and high-energy shoulder, while the low energy peaks at the L_3 and L_2 edges is not reproduced (red dashed curve in Fig. 6). The calculation fails to reproduce low energy shoulder of the XMCD major negative peak at 709 eV in L_3 XMCD spectrum. Also, the simulations for the ideal cubic BFO phase provide only one a high energy peak structure in the L_2 XMCD spectrum, however, the experimental measurements exhibit a double-peak structure.

The correct explanation of the experimental XAS and XMCD spectra is only possible by taking into account crystal imperfections, namely, oxygen vacancy. To investigate the influence of oxygen deficiency on the XAS and XMCD spectra we created an oxygen vacancy in a double supercell in the first neighborhood of the second Fe atom. We found that the presence of the oxygen vacancy decreases the valency of nearest Fe ion from 4+ to 3+ (see the corresponding discussion below). The x-ray absorption from the Fe atoms with the oxygen vacancy in close vicinity (dotted blue line in Fig. 6) contributes to the low energy peaks in the L_2 absorption and XMCD spectra. The oxygen vacancy also explain the existence of the low-energy shoulder in Fe L_3 XMCD spectrum at 709 eV.

The same conclusion can be drawn from the interpretation of the XAS and XMCD spectra at the O K edge. Fig.7 shows the experimentally measured x-ray absorption and XMCD spectra[42] (open circles) at the O K edge

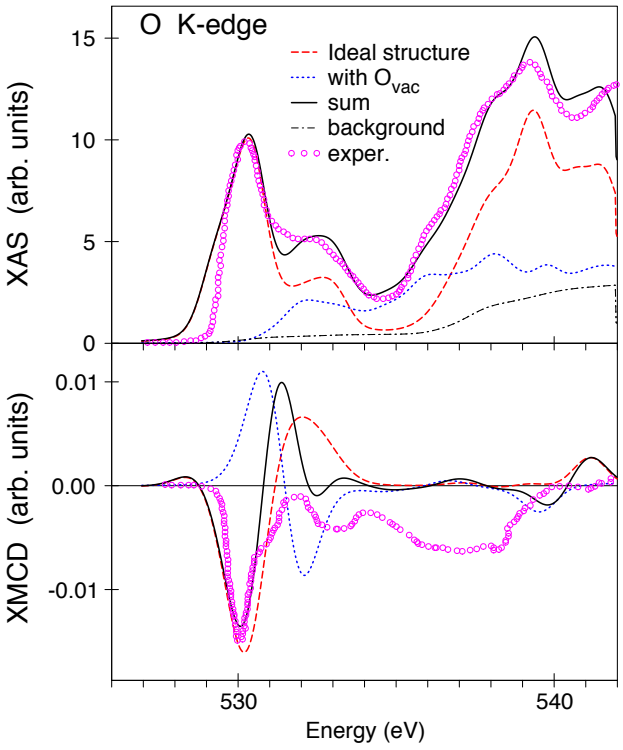

FIG. 7: (Color) Comparison between the experimental[42] (circles) x-ray absorption (upper panel) and x-ray magnetic circular dichroism (lower panel) at the O K edges of $BaFeO_3$ and the spectra calculated by the LMTO method in the GGA+U approximation (U_{eff}=3 eV) (black solid lines). Red dashed line show the spectra for ideal crystal structure, dotted blue lines present the theoretical spectra with oxygen vacancy.

in $BaFeO_3$ together with theoretically calculated spectra for the ideal crystal structure of $BaFeO_3$ (red dashed curves) and the structure with oxygen vacancy (dotted blue curves). The calculations for the ideal structure are not able to describe the high-energy shoulder of major negative XMCD peak at 531 eV, which is due to the oxygen vacancy. We can conclude that the explanation of the experimental spectra at both the Fe $L_{2,3}$ and O K edges demands the presence of crystal imperfections in $BaFeO_3$.

D. Fe valency and oxygen vacancies in $BaFeO_{3-\delta}$

To understand the vacancy formation we performed first-principles study of the Fe oxidation states in the cubic $BaFeO_3$ using a self-interaction method as it is described in Sec. II. The Fe oxidation state vary in different compounds from 2+ to 4+. For a completely oxidized BFO, one can expect a high valency, Fe^{4+}. The total energy study of the oxidation state and further comparison between BFO and $BaFeO_{3-\delta}$ can provide us with some hints concerning the electronic properties and the preferable magnetic order in BFO. The Goodenough-Kanamori rules of the 180° superexchange suggest that the interaction Fe–O–Fe can be switched from antiferromagnetic to ferromagnetic when the Fe 3d-orbital filling changes. In this context, a variety of the superexchange options, such as Fe^{4+}–O–Fe^{4+}, Fe^{3+}–O–Fe^{3+} and Fe^{4+}–O–Fe^{3+} need to be inspected. However, the Goodenough-Kanamori simplifications work robustly for insulators only. When theory deals with metallic magnetic oxide, such as the cubic BFO, the superexchange coupling does not dominate there and double exchange complicates the long-range interactions between magnetic species.

In the case of the cubic symmetry, the Fe^{4+} electronic configuration is $t_{2g}^3 e_g^1$, where the half-occupied e_g orbital has ether $d_{3z^2-r^2}$ or $d_{x^2-y^2}$ representation. For the cubic BFO case, which was treated within the LSDA-SIC model, we found that the two e_g options result in the same equilibrium volume (see Fig.8), which is substantially smaller then the experimental result (62.57 Å^3) and the volume calculated using the GGA (Fe^{2+}). Although the volume computed within the GGA is very close to the experimental value, the corresponding total energy is about 22 meV higher then the total energies of Fe^{4+} and Fe^{3+} configurations.

For the cation Fe^{3+}, its t_{2g} and e_g levels must be fully occupied in the majority spin channel. This electronic configuration yields the total-energy minimum value, which is not far above that of the Fe^{4+} ground state, as shown in Fig. 8. The calculated equilibrium volume is in a better agreement with the experimental results then the values obtained for Fe^{3+} (SIC) and Fe^{2+} (GGA) configurations. The energetics suggest that both oxidations, Fe^{4+} and Fe^{3+}, can be realized in epitaxially fabricated thin films. Configurations with other oxidation states are much higher in energy and are excluded from the further consideration.

Further, we compared the total energies of Fe^{4+} and Fe^{3+} oxidation states in the presence of oxygen vacancies. For $\delta = 0.03$ the total energies in the equilibrium volumes are almost the same (see Fig. 8). Thus, the vacancy formation lowers the energy of the Fe^{3+} oxidation state, which agrees with our interpretation of the XAS and XMCD experiments. In a real BFO sample, both oxidation states can coexist, which is as well evident from our XAS and XMCD simulations. In Fig. 8 we present the total energy for a mixed configuration, which is lower then the others in a particular concentration range.

As next, we investigated the impact of oxygen vacancies on magnetic properties of the BFO. The oxygen vacancies were simulated within a $4 \times 1 \times 1$ supercell, in which one oxygen site was occupied by an vacancy with a given probability. The disorder was simulated using the CPA method. The use of the supercell enables to take into account short-range effects in a simple manner, which can take place in real materials. Results for the exchange interaction, computed in this supercell and $\delta = 0.25$, are presented in Fig. 9. While the exchange interaction between the Fe^{4+} cations is strong and positive,

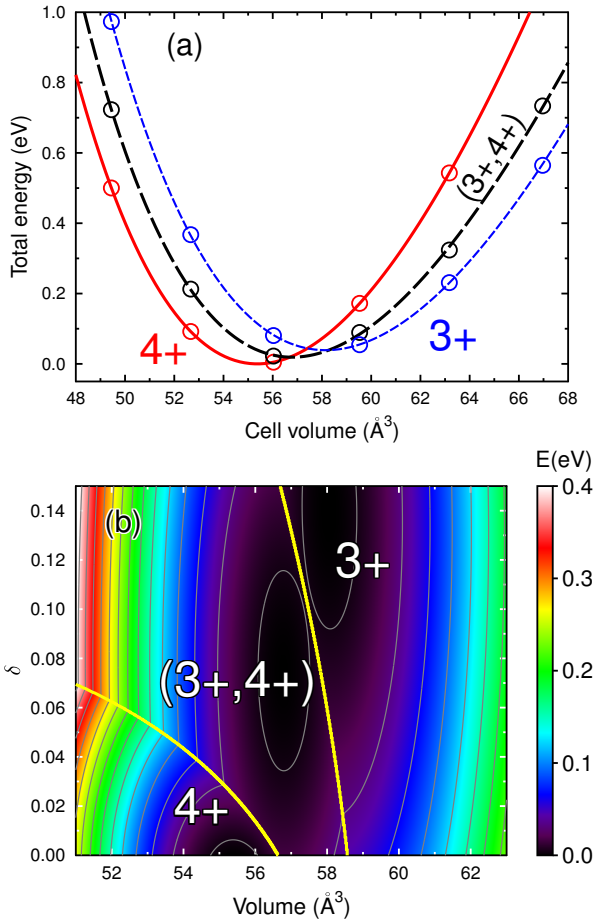

FIG. 8: (Color) The total energies of $BaFeO_{3-\delta}$, calculated using the LSDA-SIC option for the Fe^{4+}, Fe^{3+}, and a combination of them 1:1. Energies as functions of the volume without oxygen vacancies (a). Total energy as a function of volume and δ (b).

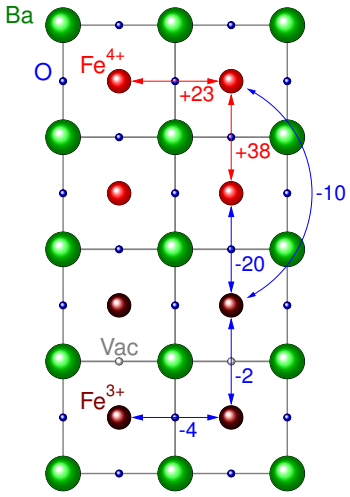

FIG. 9: (Color) Exchange interaction in the $BaFeO_{2.75}$ simulated in a $4 \times 1 \times 1$ supercell.

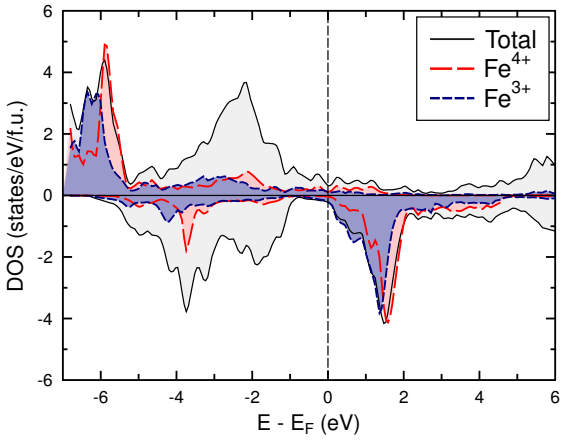

FIG. 10: (Color) DOS of the $BaFeO_{2.75}$ simulated in a $4\times1\times1$ supercell.

it is week and negative between the Fe^{3+} atoms. The reason for this can be understood from the DOS, shown in Fig. 10. Because of the vacancy (missing oxygen), the $3d$ states of the Fe^{3+} are more localized (in particular the e_g states) and are shifted down in energy. This increases the tendency to an antiferromagnetic coupling. The coupling between the atoms in different oxidation states is as well antiferromagnetic and very strong due to the large difference of the DOS. This funding agrees with the main conclusions of S. Mori, who first developed a model for the magnetic structure of $BaFeO_x$.[43]

Depending on the vacancy concentration and their distribution, the non-trivial exchange interaction in $BaFeO_{3-\delta}$ can results in various magnetic orders. In Fig. 11, we show the change of critical temperature with the oxygen vacancy concentration simulated within the MFA and RPA approaches. The negative T_C means here the absence of the ferromagnetic order (either antiferromagnetic or non-collinear). Thus, for a moderate vacancy concentration δ of 0.15 – 0.20, T_C lies in the experimental range of 250 – 100 K.

IV. SUMMARY

In this work we studied electronic and magnetic properties of a cubic $BaFeO_3$ within a DFT framework using a GGA and a GGA+U approaches. We predicted that the $BaFeO_3$ in an ideal stoichiometric cubic structure should be half-metallic and ferromagnetic with a high Curie temperature of 700 – 900 K. However, this finding disagrees the experiments, which found that the compound has a T_C far below the room temperature. To understand this discrepancy we simulated XAS and XMCD spectra comparing the theoretically obtained results with available experimental data. Herewith, we varied the chemical composition, structural and electronic parameters to obtain a better agreement with experiments. Our sim-

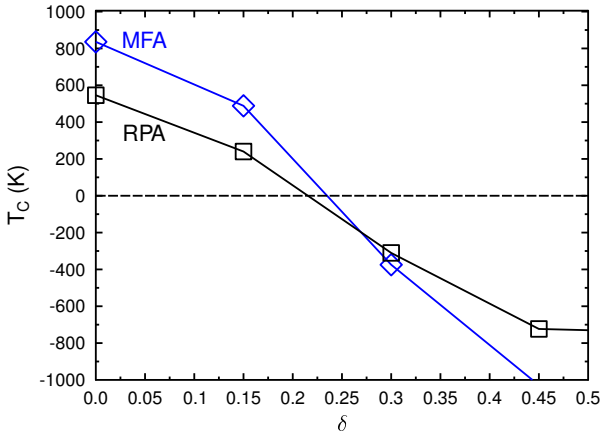

FIG. 11: (Color) Critical temperature T_C in $BaFeO_{3-\delta}$ as a function of oxygen vacancy concentration δ. Here, the negative T_C means the absence of the ferromagnetic order.

ulations showed that the experimental observations can be explained by oxygen vacancies, which can be present in real BFO samples. Thereby, Fe atoms near an oxygen vacancy change their oxidation state from 4+ to 3+. Thus, a real cubic $BaFeO_3$ may contain both Fe^{4+} and Fe^{3+} cations, which explains the experimentally observed double peak structure in XAS and XMCD spectra. Further, we found that oxygen vacancies can substantially reduce the Curie temperature of a cubic BFO or even change the ferromagnetic order to an antiferromagnetic one or a non-collinear structure. Responsible for this is a strong antiferromagnetic exchange coupling between Fe atoms of different oxidation states. This result provides a clear route to fabricate a robust ferromagnetic $BaFeO_3$ with a high Curie temperature by reducing the amount of oxygen vacancies and stabilizing it in the cubic structure.

V. ACKNOWLEDGMENTS

This work is supported by the DFG within the Collaborative Research Center *Sonderforschungsbereich* SFB 762, 'Functionality of Oxide Interfaces'.

* Electronic address: igor.maznichenko@physik.uni-halle.de

[1] V. Garcia, M. Bibes, L. Bocher, S. Valencia, F. Kronast, A. Crassous, X. Moya, S. Enouz-Vedrenne, A. Gloter, D. Imhoff, et al., Science **327**, 1106 (2010).

[2] S. Valencia, A. Crassous, L. Bocher, V. Garcia, X. Moya, R. Cherifi, C. Deranlot, K. Bouzehouane, S. Fusil, A. Zobelli, et al., Nature materials **10**, 753 (2011).

[3] H. L. Meyerheim, F. Klimenta, A. Ernst, K. Mohseni, S. Ostanin, M. Fechner, S. Parihar, I. V. Maznichenko, I. Mertig, and J. Kirschner, Phys. Rev. Lett. **106**, 087203 (2011).

[4] L. Martin and R. Ramesh, Acta Materialia **60**, 2449 (2012).

[5] D. Pantel, S. Goetze, D. Hesse, and M. Alexe, Nature materials **11**, 289 (2012).

[6] S. Chakraverty, T. Matsuda, N. Ogawa, H. Wadati, E. Ikenaga, M. Kawasaki, Y. Tokura, and H. Hwang, Applied Physics Letters **103**, 142416 (2013).

[7] N. Hayashi, T. Yamamoto, H. Kageyama, M. Nishi, Y. Watanabe, T. Kawakami, Y. Matsushita, A. Fujimori, and M. Takano, Angewandte Chemie **123**, 12755 (2011).

[8] B. Ribeiro, R. Borges, R. da Silva, N. Franco, P. Ferreira, E. Alves, B. Berini, A. Fouchet, N. Keller, and M. Godinho, Journal of Applied Physics **111**, 113923 (2012).

[9] C. Callender, D. P. Norton, R. Das, A. Hebard, and J. D. Budai, Applied Physics Letters **92**, 012514 (2008).

[10] H. A. Jahn and E. Teller, Royal Society of London Proceedings Series A **161**, 220 (1937).

[11] J. Rodríguez-Carvajal, M. Hennion, F. Moussa, A. H. Moudden, L. Pinsard, and A. Revcolevschi, Phys. Rev. B **57**, R3189 (1998).

[12] Q. Huang, A. Santoro, J. W. Lynn, R. W. Erwin, J. A. Borchers, J. L. Peng, K. Ghosh, and R. L. Greene, Phys. Rev. B **58**, 2684 (1998).

[13] J. Hemberger, A. Krimmel, T. Kurz, H.-A. Krug von Nidda, V. Y. Ivanov, A. A. Mukhin, A. M. Balbashov, and A. Loidl, Phys. Rev. B **66**, 094410 (2002).

[14] N. Hayashi, T. Yamamoto, A. Kitada, A. Matsuo, K. Kindo, J. Hester, H. Kageyama, and M. Takano, Journal of the Physical Society of Japan **82** (2013).

[15] D. Fuks, Y. Mastrikov, E. Kotomin, and J. Maier, Journal of Materials Chemistry A **1**, 14320 (2013).

[16] T. Li, Z. Feng, C. Jing, F. Hong, S. Cao, and J. Zhang, Eur. Phys. J. B **86**, 414 (2013).

[17] B. Ribeiro, M. Godinho, C. Cardoso, R. Borges, and T. Gasche, Journal of Applied Physics **113**, 083906 (2013).

[18] M. Mostovoy, Physical review letters **94**, 137205 (2005).

[19] Z. Li, R. Laskowski, T. Iitaka, and T. Tohyama, Physical Review B **85**, 134419 (2012).

[20] Z. Li, T. Iitaka, and T. Tohyama, Physical Review B **86**, 094422 (2012).

[21] M. Lüders, A. Ernst, W. M. Temmerman, Z. Szotek, and P. J. Durham, Journal of Physics: Condensed Matter **13**, 8587 (2001).

[22] J. P. Perdew, K. Burke, and M. Ernzerhof, Phys. Rev. Lett. **77**, 3865 (1996).

[23] J. P. Perdew and A. Zunger, Phys. Rev. B **23**, 5048 (1981).

[24] M. Lüders, A. Ernst, M. Däne, Z. Szotek, A. Svane, D. Ködderitzsch, W. Hergert, B. L. Györffy, and W. M. Temmerman, Phys. Rev. B **71**, 205109 (2005).

[25] V. I. Anisimov, J. Zaanen, and O. K. Andersen, Phys. Rev. B **44**, 943 (1991).

[26] A. I. Liechtenstein, M. I. Katsnelson, V. P. Antropov, and V. A. Gubanov, Journal of Magnetism and Magnetic Materials **67**, 65 (1987).

[27] S. Tyablikov, *Methods in the quantum theory of magnetism* (Plenum Press, 1967).

[28] G. Fischer, M. Dane, A. Ernst, P. Bruno, M. Luders,

Z. Szotek, W. Temmerman, and W. Hergert, Physical Review B (Condensed Matter and Materials Physics) **80**, 014408 (2009).
[29] C. Etz, I. V. Maznichenko, D. Böttcher, J. Henk, A. N. Yaresko, W. Hergert, I. I. Mazin, I. Mertig, and A. Ernst, Phys. Rev. B **86**, 064441 (2012).
[30] B. L. Gyorffy, Phys. Rev. B **5**, 2382 (1972).
[31] T. Oguchi, K. Terakura, and N. Hamada, Journal of Physics F: Metal Physics **13**, 145 (1983).
[32] B. L. Gyorffy, A. J. Pindor, J. Staunton, G. M. Stocks, and H. Winter, Journal of Physics F: Metal Physics **15**, 1337 (1985).
[33] O. K. Andersen, Phys. Rev. B **12**, 3060 (1975).
[34] V. V. Nemoshkalenko, A. E. Krasovskii, V. N. Antonov, V. N. Antonov, U. Fleck, H. Wonn, and P. Ziesche, **120**, 283 (1983).
[35] V. N. Antonov, H. A. Dürr, Y. Kucherenko, L. V. Bekenov, and A. N. Yaresko, Phys. Rev. B **72**, 054441 (2005).
[36] V. N. Antonov, O. Jepsen, A. N. Yaresko, and A. P. Shpak, J. Appl. Phys. **100**, 043711 (2006).
[37] V. N. Antonov, A. N. Yaresko, and O. Jepsen, Phys. Rev. B **81**, 075209 (2010).
[38] X. D. Zou, S. Hovmöller, M. Parras, J. M. González-Calbet, M. Vallet-Reg, and J. C. Grenier, Acta Crystallographica Section A **49**, 27 (1993).
[39] J. P. Perdew and Y. Wang, Phys. Rev. B **45**, 13244 (1992).
[40] M. Pajda, J. Kudrnovský, I. Turek, V. Drchal, and P. Bruno, Phys. Rev. B **64**, 174402 (2001).
[41] V. I. Anisimov, F. Aryasetiawan, and A. I. Lichtenstein, Journal of Physics: Condensed Matter **9**, 767 (1997).
[42] T. Tsuyama, T. Matsuda, S. Chakraverty, J. Okamoto, E. Ikenaga, A. Tanaka, T. Mizokawa, H. Y. Hwang, Y. Tokura, and H. Wadati, Phys. Rev. B **91**, 115101 (2015).
[43] S. Mori, Journal of the Physical Society of Japan **28**, 44 (1970).